Journal of Power Sources 260 (2014) 6–11

Contents lists available at ScienceDirect

Journal of Power Sources

journal homepage: www.elsevier.com/locate/jpowsour

Morphology-controlled cactus-like branched anatase TiO_2 arrays with high light-harvesting efficiency for dye-sensitized solar cells

Wu-Qiang Wu [a], Hua-Shang Rao [a], Hao-Lin Feng [a], Xin-Dong Guo [b], Cheng-Yong Su [a], Dai-Bin Kuang [a,*]

[a] MOE Key Laboratory of Bioinorganic and Synthetic Chemistry, KLGHEI of Environment and Energy Chemistry, State Key Laboratory of Optoelectronic Materials and Technologies, School of Chemistry and Chemical Engineering, Sun Yat-sen University, Guangzhou 510275, PR China
[b] Guangzhou Quality Supervision and Testing Institute, Guangzhou 510110, PR China

HIGHLIGHTS

- Cactus-like branched anatase TiO_2 arrays were prepared by hydrothermal method.
- The TiO_2 NW arrays consist of the oriented NW or NS stem and a host of NR branches.
- Different TiO_2 NW arrays based DSSCs were investigated by IV, EIS and CIMPS/IMVS.
- DSSCs based on 7 μm long TiO_2 NW arrays yielded a power conversion efficiency of 6.43%.

GRAPHICAL ABSTRACT

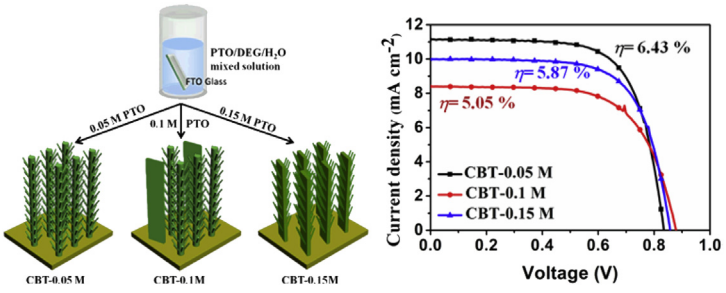

ARTICLE INFO

Article history:
Received 23 December 2013
Received in revised form
10 February 2014
Accepted 27 February 2014
Available online 12 March 2014

Keywords:
Cactus-like branched TiO_2
Nanowire arrays
Morphologically-controllable
Dye-sensitized solar cells
Light-harvesting

ABSTRACT

The present work establishes a facile process for one-step hydrothermal growth of vertically aligned anatase cactus-like branched TiO_2 (CBT) arrays on a transparent conducting oxide (TCO) substrate. Various CBT morphologies are obtained by adjusting the potassium titanium oxide oxalate (PTO) reactant concentration (from 0.05 M to 0.15 M) and this yields a morphologically-controllable branched TiO_2 arrays geometry. The CBT arrays consist of a vertically oriented nanowire (NW) or nanosheet (NS) stem and a host of short nanorod (NR) branches. The hierarchical CBT arrays demonstrate their excellent candidatures as photoanodes, which are capable of exhibiting high light-harvesting efficiency in dye-sensitized solar cells (DSSCs). Consequently, DSSCs based on 7 μm long optimized CBT arrays (0.05 M PTO), which are assembled with high density and high aspect-ratio NR branches, exhibit an impressive power conversion efficiency of 6.43% under AM 1.5G one sun illumination. The high performance can be attributed to the prominent light-harvesting efficiency, resulting from larger surface area and superior light-scattering capability.

1. Introduction

Ever since the Grätzel-typed dye-sensitized solar cells (DSSCs) were reported in 1991, they have attracted tremendous attentions in scientific and technological field due to their high power conversion efficiency, low cost as well as facile fabrication process [1–3]. The key components of a DSSC include dye sensitizers, redox electrolytes, nanoporous TiO_2 films, and Pt counter electrodes [4–9]. Of particular interest is the TiO_2 layer, which serves as the transport media for photo-generated electrons and plays a vital role in affecting light-harvesting and charge-collection efficiency of photoanodes [10]. Hence, continuous efforts have been made on

* Corresponding author. Tel./fax: +86 20 84113015.
E-mail address: kuangdb@mail.sysu.edu.cn (D.-B. Kuang).

http://dx.doi.org/10.1016/j.jpowsour.2014.02.107
0378-7753/

the development of a more effective TiO_2 photoanode. In many occasions, well-aligned TiO_2 nanostructures, such as nanorod (NR), nanowire (NW), nanotube (NT), have been widely used as a replacement for stereotyped nanoparticulate mesoporous TiO_2 film in DSSCs photoanodes [11–21]. In particular, one-dimensional vertically aligned TiO_2 arrays such as NWs have been proven to be an ideal kind of photoanode to accelerate electron transport through providing a direct electric transport pathway and thus act as more efficient charge collectors than the randomly packed nanoparticle (NP) counterparts [22].

Up till now, several methods have been developed to fabricate a wide range of TiO_2 NW arrays with various morphologies directly on TCO substrates. In particular, hydrothermal growth has been identified as the most promising solution-processed technology. Over the years, the control over the crystallography and geometry of the nanowires has been drastically improved. For instance, the crystal phase (rutile or anatase), length, diameter as well as the degree of hierarchy order can be adjusted by selecting appropriate hydrothermal parameters [23–26]. Especially worth to note is the fact that the anatase TiO_2 NW with long length or dendritic NR branches is emerging and gradually overwhelming the rutile TiO_2 rivals when applied in photovoltaic cells [27,28]. Generally, anatase TiO_2 possesses better electron transport, lower charge recombination rate, higher surface area and superior optical transparency than rutile counterpart [29]. Very thin anatase TiO_2 NR arrays on TCO substrate have been prepared via corroding the Ti-sputtered FTO glass in alkali solution [30]. Recently, a facile hydrothermal growth route was firstly presented in our previous report, where the hierarchical long anatase TiO_2 NW was grown directly on FTO glass in mixed solution containing potassium titanium oxide oxalate dehydrate (PTO), diethylene glycol (DEG) and water [12]. It is worth noting that configuring the branched TiO_2 NW framework with a large number of dendritic NR branches is beneficial to further enlarge the surface area and thus promote the dye uptakes while at the same time preserves the superior electron transport property [12,31]. To the best of our knowledge, there have been no reports on the fabrication of various cactus-like TiO_2 NW arrays architectures with controllable morphologies by simply adjusting the PTO reactant concentration and their application as photoanodes in DSSCs.

Herein, we report various novel hierarchical anatase cactus-like branched TiO_2 (CBT) NW arrays directly grown on a TCO substrate in the PTO/DEG/water system. Compared with previous work, [12] we herein optimized the DEG/H_2O ratio into another value (1:5) and carefully adjusted the PTO concentration in the range from 0.05 M to 0.15 M. Consequently, three different types of CBT arrays (CBT − 0.05 M, CBT − 0.1 M and CBT − 0.15 M) are successfully prepared and used as photoanodes in DSSCs and their effects on the cell performance are investigated in details. Relative to previous work and other related works, the advantages of present fabrication technique lie in the controllable synthesis of hierarchical TiO_2 nanowires with various trunks morphologies and branches distributions, which possess distinct photovoltaic characteristics. Accordingly, the vertically aligned CBT arrays exhibit efficient electron transport and showcase their candidature as an excellent light harvester in DSSCs.

2. Experimental

2.1. Synthesis of various TiO_2 nanoarrays

First, different amount of potassium titanium oxide oxalate dehydrate (PTO) was dissolved in mixture solvent containing 2.5 mL deionized water and 17.5 mL diethylene glycol (DEG). After stirring for 30 min, the mixture solution was transferred to a 50 mL Teflon-lined stainless steel autoclave. Then the TiO_2-coated FTO glass (a 100 nm thick TiO_2 compact layer on FTO glass is obtained by spin-coating of the synthesized TiO_2 colloid solution [32] followed by 30 min heat treatment at 500 °C in ambient air) was placed at an angle against the wall of the Teflon-liner with the conducting side facing down. The hydrothermal synthesis was carried out at 180 °C for 9 h. After the reaction, the autoclave was cooled to room temperature naturally and then the as-prepared CBT arrays were taken out and rinsed with deionized water and ethanol several times and then heated in air at 550 °C for 1 h to remove the residual DEG and increase crystallinity. To control the morphology of CBT arrays, the concentration of PTO reactant was varied from 0.05 M to 0.15 M. Specifically, three different types of CBT arrays with distinguished morphologies were synthesized by using 0.05 M, 0.1 M or 0.15 M PTO, respectively, and the resulting samples were designated as CBT − 0.05 M, CBT − 0.1 M and CBT − 0.15 M, respectively.

2.2. Preparation of TiO_2 photoanodes and DSSCs assembly

The as-prepared CBT arrays on FTO glass were used as photoelectrodes for DSSCs. Prior to dye sensitization, the films were immersed into a 40 mM $TiCl_4$ aqueous solution at 70 °C for 30 min. After rinsing with water and ethanol, $TiCl_4$ treated CBT arrays were sintered in air at 520 °C for 30 min. After cooling down to 80 °C, the CBT films were immersed into 0.5 mM N719 dye in acetonitrile/*tert*-butanol (1:1 v/v) and kept for 20 h at room temperature. Then the TiO_2 photoanode was assembled with Pt sheet counter electrode in a sandwich type and the electrolyte is injected into the space between them. The preparation of I^-/I_3^- based liquid electrolyte is the same with our previous report [33]. The active area of the CBT arrays film is approximately 0.16 cm^2.

2.3. Characterizations

The Field emission scanning electron microscopy (FE-SEM, JSM-6330F) and transmission electron microscope (TEM, JEOL-2010 HR) were used to characterize the intrinsic morphology and structure of CBT arrays. The phase purity of the samples was characterized by X-ray diffraction (XRD, Bruker D8 Advance) using Cu Kα radiation (λ = 1.5418 Å). The photovoltaic performance characteristics including J_{sc}, V_{oc}, *FF* and η were measured using a Keithley 2400 source meter under simulated AM 1.5 G illumination (100 mW cm^{-2}) provided by a solar light simulator (Oriel, Model: 91192). The incident light intensity was calibrated with a NREL-calibrated Si solar cell. The IPCE spectra were measured as a function of wavelength from 380 to 800 nm on a Spectral Products DK240 monochromator. The amount of dye uptakes (the adsorbed dye on TiO_2 films was desorbed in 0.1 M NaOH aqueous solution) and the reflectance spectra of the TiO_2 films were measured by using a UV/vis-NIR spectrophotometer (UV-3150). The electrochemical impedance spectra (EIS) were conducted on an electrochemical workstation (Zahner, Zennium) at a bias potential of −0.85 V in the dark with the frequency range from 10 mHz to 1 MHz. The magnitude of the alternative signal was 10 mV. Intensity-modulated photocurrent/photovoltage spectroscopy (IMPS/IMVS) measurements were also carried out on an electrochemical workstation (Zahner, Zennium). The frequency range is set from 1 KHz to 0.1 Hz.

3. Results and discussion

3.1. Preparation procedure, XRD patterns and intrinsic morphologies of various CBT arrays films

Fig. 1 displays schematic diagram of various novel hierarchical anatase cactus-like branched TiO_2 (CBT) NW arrays directly grown on a TCO substrate, which are based on careful adjustment of PTO

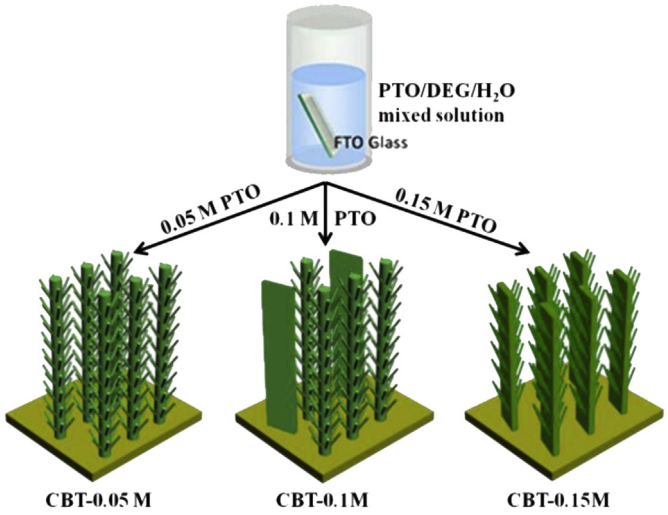

Fig. 1. Schematic diagram of one-step synthesis of various vertically-aligned cactus-like branched TiO_2 nanowire arrays on FTO glass under the condition of different PTO reactant concentration (0.05 M, 0.1 M and 0.15 M).

reactant concentration in the precursor growth solution, and eventually leading to formation of interesting cactus-like morphologies consisting of different TiO_2 backbones (1D NW or 2D NS) and a large number of dendritic NR branches.

The hierarchical cactus-like branched TiO_2 nanostructure arrays are synthesized via a one-step hydrothermal reaction in the PTO/DEG/water system. The XRD pattern (Fig. S1) indicates that these three as-prepared samples can be indexed as pure anatase TiO_2. Specifically, the sharp peaks located at 25.4°, 48.1°, 54.6° and 55.3° can be observed, corresponding to the (101), (200), (105), (211) crystal planes of anatase TiO_2, respectively. Fig. 2 shows the FESEM images of various CBT arrays derived from different PTO concentrations (0.05 M, 0.1 M and 0.15 M) at low and high magnifications. Obviously, the morphologies of the CBT arrays are strongly dependent on the PTO precursor concentration. The lengths of all three samples are similar (~7 μm) with vertically oriented 1D geometry grown almost perpendicularly from the FTO substrate (Fig. S2). CBT arrays comprised of a long 1D NW stem and numerous NR branches are obtained at a PTO concentration of 0.05 M (CBT – 0.05 M, Fig. 2a and b). In this case, the NR branches with high-density and high aspect-ratio can provide high porosity and a larger surface area. With an increase in PTO concentration to 0.15 M, the morphology of CBT arrays witness significant change, in which a fully-developed arrays consisting of 2D NS backbones and well-distributed NR branches can be observed (CBT – 0.15 M, Fig. 2e and f). When using 0.1 M PTO, a transitional intermediate structure composed of a large proportion of branched NWs and a small portion of smooth NS stems can be noticed (CBT – 0.1 M, Fig. 2c and d). Thus, it can be concluded that the variation of PTO concentration greatly affects the morphology of CBT arrays, which can be ascribed to the different crystal growth rate and reorganization, leading to the formation of cactus-like structures and allowing for the control over the shape of both stems and branches. 0.05 M PTO has been proved to be the suitable concentration that enables slow hydrolysis rate to form tree-like TiO_2 NWs comprised of long NW trunks and short NR branches [12]. However, a higher PTO precursor concentration will facilitate the hydrolysis rate and promote the nucleation and crystallization of TiO_2 in a short period of time, eventually resulting in the formation of larger-sized TiO_2 NS backbones decorated with NR branches.

The morphological and structural properties of two well-developed CBT arrays (CBT – 0.05 M and CBT – 0.15 M) are further characterized by TEM analysis. As shown in Fig. 3b, a large number of NR branches with high density and high aspect-ratio (8–10 nm in diameter and 150 nm–300 nm in length) are uniformly grown on the long NW stem (approximately 7 μm in length and 100 nm in diameter) of CBT – 0.05 M. The magnified image in Fig. 3c reveals that the slender and interlaced NR branches can not only enhance the surface area for dye adsorption, but also generate many small mesopores with a high porosity for sufficient electrolyte infiltration. As for the CBT – 0.15 M, the major distinction lies in the large-sized 2D NS backbone (Fig. 3e), where a relatively smaller number of NR branches selectively germinates on the surface of both wing sides (Fig. 3f).

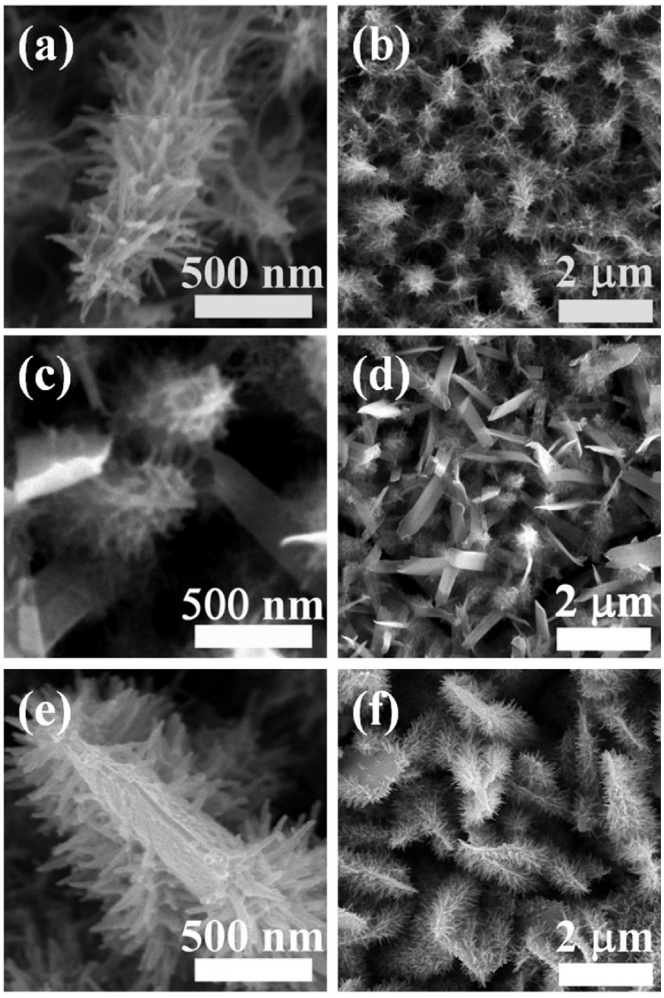

Fig. 2. FESEM images of CBT arrays at low and high magnification: (a, b) CBT – 0.05 M; (c, d) CBT – 0.1 M; (e, f) CBT – 0.15 M.

3.2. Photovoltaic performance and incident photon-to-current conversion efficiency of DSSCs based on various CBT arrays photoelectrodes

To illustrate the influences of NW arrays geometry on photovoltaic performance of DSSCs, the aforementioned three types of CBT arrays were applied as photoanodes in DSSCs. Fig. 4a shows the typical photocurrent density–photovoltage (J–V) curves of DSSCs based on these CBT arrays. The detailed photovoltaic parameters are summarized in Table 1. As anticipated, the solar cells based on CBT – 0.05 M photoanodes attain the highest power conversion efficiency of 6.43%, which is higher than that of CBT – 0.15 M

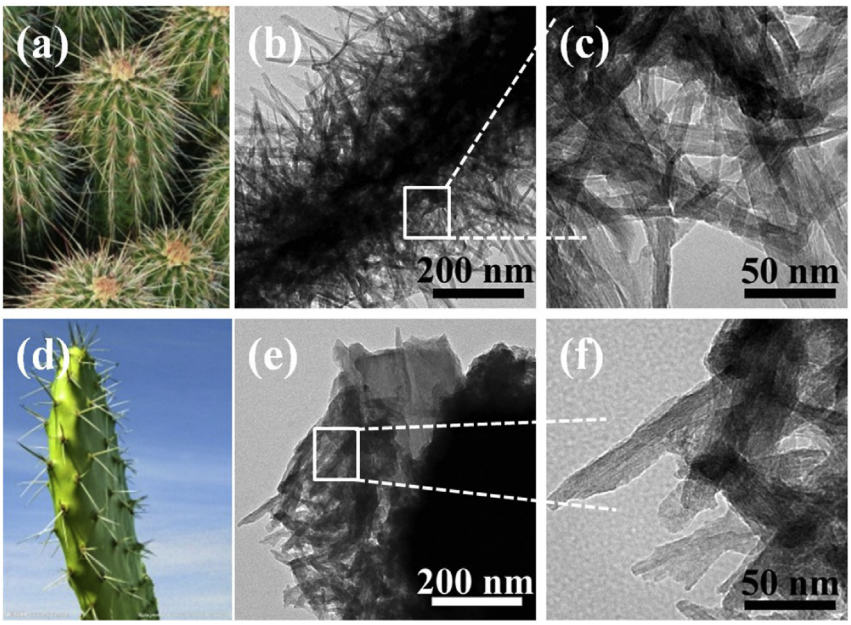

Fig. 3. (a, d) The corresponding images of two kinds of representative cacti; TEM images of well-developed CBT arrays at different magnifications: (b, c) CBT – 0.05 M; (e, f) CBT – 0.15 M.

(5.87%) and CBT – 0.1 M arrays (5.05%). The dye-loading amounts of photoanodes derived from CBT – 0.05 M, CBT – 0.1 M and CBT – 0.15 M films are 63.49, 42.33 and 52.03 nmol cm^{-2}, respectively. The largest amount of dye uptakes for CBT – 0.05 M film can be attributed to the extremely high aspect-ratio long NW stem and a high density of dendritic NR branches, as confirmed by SEM and TEM analyses. While the smallest amount of dye uptakes for CBT – 0.1 M film should be primarily due to its intermediate structure with a certain number of smooth nanosheets and a portion of hierarchical nanowires with fewer branches modification. Fig. 4b shows the IPCE spectra of DSSCs based on various CBT arrays photoanodes as a function of wavelength from 380 to 800 nm. The peak values of IPCE spectra at around 530 nm are 67.5%, 51.6% and 57.8% for CBT – 0.05 M, CBT – 0.1 M and CBT – 0.15 M, respectively, which is in good consistent with the variation tendency of the corresponding J_{sc} of DSSCs. Notably, a red-shift phenomenon especially at longer wavelength (600–750 nm) can be obviously observed for the DSSCs based on the well-developed CBT – 0.05 M and CBT – 0.15 M films with well-rounded NR branches, which can effectively scatter the incident light and utilize them efficiently as compared to that of transitional intermediate structure of CBT – -0.1 M films. This notion can be well supported by the diffused reflectance spectra (Fig. S3), in which better diffused reflectance capability of the CBT – 0.05 M film and CBT – 0.15 M film than that of CBT – 0.1 M film can be clearly observed, indicating enhanced scattering of incident light at the well-developed porous hierarchical branched framework. In short, we conclude the higher efficiencies of CBT – 0.05 M based cells primarily resulted from higher J_{sc}, which can be related to several contributions: (a) a larger surface area and consequently a higher dye-loading; (b) an enhanced light scattering property for efficient light-harvesting; (c) an interlaced and interconnected framework with a high porosity for effective electrolyte penetration. In contrast, the inferior light scattering and dye uptakes capability for CBT – 0.1 M restricted the efficiency to the lowest level (5.05%) among all three kinds of cells.

3.3. Electrochemical impedance spectroscopic studies of DSSCs based on various CBT arrays photoelectrodes

On the other hand, it is interesting to point out that V_{oc} values obtained from three devices are different, for which a different recombination rate and thus discriminative electron lifetime within the cells is expected. For this, the EIS spectra in Fig. 5 are utilized to further understanding this behavior. The fitted recombination

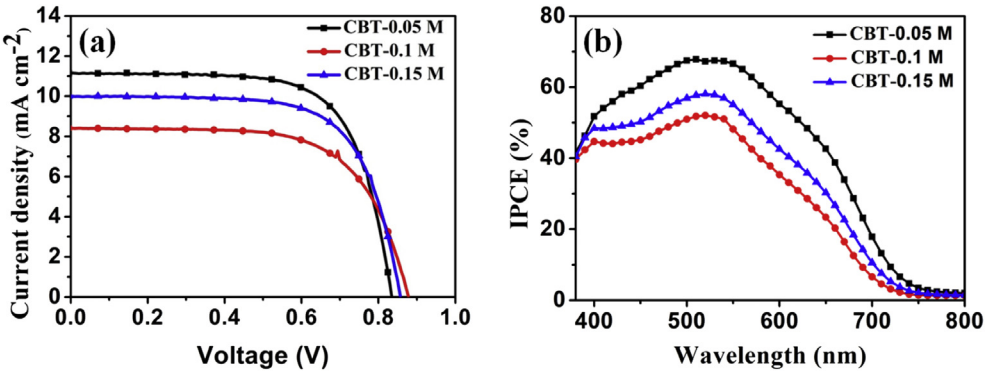

Fig. 4. (a) *J–V* characteristics and (b) IPCE spectra of DSSCs based on various CBT arrays photoanodes.

Table 1
Photovoltaic performance of DSSCs based on different CBT arrays photoelectrodes with a thickness of 7 μm.

DSSCs	J_{sc}/mA cm^{-2}	V_{oc}/mV	η/%	*FF*	Adsorbed dye/ nmol cm^{-2}
CBT − 0.05 M	11.15	835	6.43	0.69	63.49
CBT − 0.1 M	8.40	878	5.05	0.69	42.33
CBT − 0.15 M	10.00	857	5.87	0.68	52.03

resistance (R_2) and electron lifetime (τ_r) are summarized in Table S1. In general, R_2 represents the charge transfer resistance at the interface of TiO_2/dye/electrolyte [34]. Typically, smaller R_2 means that it is more easy for the photo-injected electrons on conduction band of TiO_2 to recombine with oxidized species in dye or electrolyte. In this case, much more serious charge recombination within the cells would happen. Clearly, there is a huge difference regarding the R_2 values of all three devices owing to the different electrode structures. The smallest R_2 value (179.3 Ω) of DSSCs based on CBT − 0.05 M indicates a more serious recombination occurred within cells based on such arrays, which possess relatively complicated electron transfer pathway owing to a high density of interconnected NR branches. In terms of electron lifetime, DSSCs based on CBT − 0.1 M (composed of branched NW and smooth NS) showcase longest τ_r of 0.160 s, indicating the slowest charge recombination. As anticipated, the τ_r of the CBT − 0.05 M cell (0.127 s) is the shortest one among all cells, which is mainly because the larger surface area of CBT − 0.05 M film and thus providing much more trapping sites, leading to a more serious charge recombination of photo-generated electrons with I_3^- in the electrolyte and thus lowest V_{oc} can be obtained.

3.4. Charge transfer and recombination dynamic analysis of DSSCs based on various CBT arrays photoelectrodes

Intensity-modulated photocurrent/photovoltage spectroscopy (IMPS/IMVS) measurements are further carried out to reveal the intrinsic electron transport and recombination properties within DSSCs. Fig. 6 depicts the electron transport time (τ_d) and electron lifetime (τ_r) for three cells, where τ_d and τ_r represent electron transit time across the photoanode films and recombination time of electrons with I_3^- in the electrolyte, respectively. These two parameters are derived from the following equations as $\tau_d = 1/2\pi f_d$ or $\tau_r = 1/2\pi f_r$, where f_d or f_r is the characteristic minimum frequency of the IMPS and IMVS imaginary component, respectively [35]. Obviously, DSSCs based on CBT − 0.1 M arrays photoanode showcase shortest transport time and longest electron lifetime than other two CBT arrays

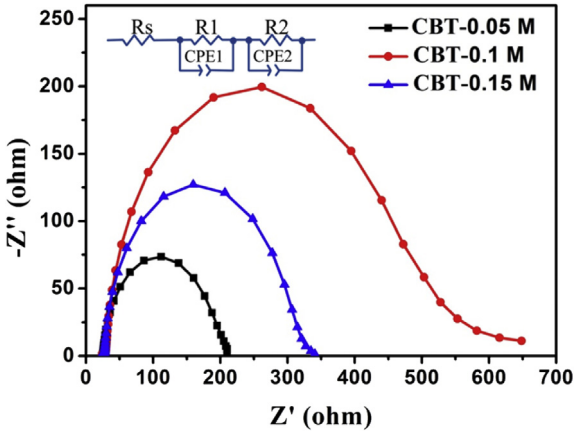

Fig. 5. EIS spectra of DSSCs based on various CBT arrays photoanodes.

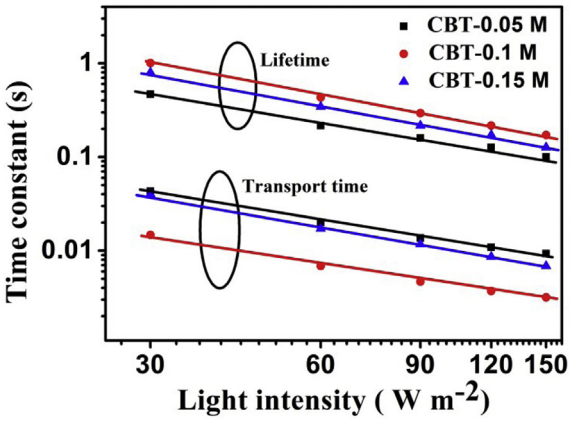

Fig. 6. IMPS/IMVS results of DSSCs based on various CBT arrays photoanodes.

based counterparts, indicating faster electron transport and slower electron recombination rate for the former. Thus, we can conclude that the electron transport will be prolonged and the recombination rate will be aggravated for the well-developed hierarchical branched arrays (CBT − 0.05 M and CBT − 0.15 M) with complicated and interconnected branched architectures, and thus V_{oc} reduction would be expected. This result is in good consistent with EIS analysis. However, the significant increase in J_{sc} of DSSC based on these two structures is not deleteriously compensated by a reduction in V_{oc}, rather it still gives enough place for the promising improvement of overall power conversion efficiency.

To gain better insight into the electron transport within various DSSCs, the calculated electron diffusion coefficients (D_n; $D_n = d^2/(4\tau_d)$) [36] for all three cells were are plotted in Fig. 7 as a function of various light intensities. One can notice that the D_n curve of the CBT − 0.1 M derived DSSC lies above that of other two kinds of CBT arrays derived DSSCs, again confirming faster electron transit capability of the cells based on CBT − 0.1 M arrays photoanodes owing to its transitional intermediate structure composed of a large proportion of branched NWs and a small portion of smooth NS, leading to the lowest surface area and thus low dye-loading amount, in which fewer surface trapping sites and defects within these cells and thus facilitated charge transfer, while other two kinds of well-developed CBT arrays (CBT − 0.05 M and CBT − 0.15 M) possess relatively inferior electron transport properties due

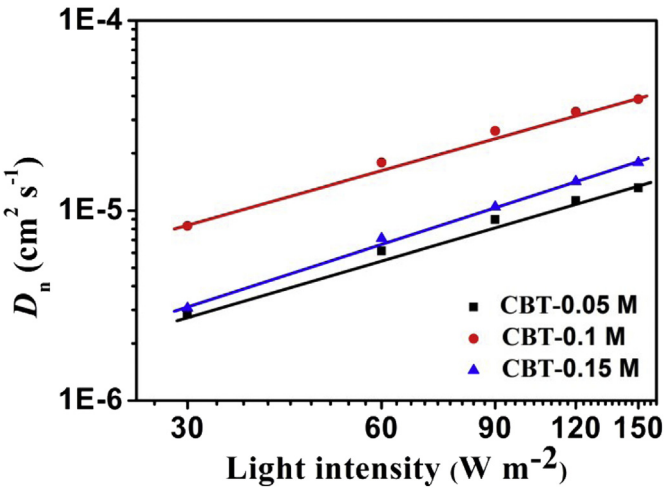

Fig. 7. Electron diffusion coefficients of DSSCs based on various CBT arrays photoanodes.

to their well-rounded hierarchical branched structures, and this observation is in good concurrence with IMPS measurements.

4. Conclusions

In summary, novel morphology-controlled 3D hierarchical cactus-like branched anatase TiO_2 arrays on TCO substrate are synthesized via a simple one-step hydrothermal method. These newly designed CBT arrays exhibit the optimized optical (prominent light scattering) and photoelectric (fast electron transport and efficient charge collection) properties. Consequently, DSSCs based on 7 μm long CBT arrays (CBT – 0.05 M) assembled with high density and high aspect-ratio NR branches exhibit a promising power conversion efficiency of 6.43%. The high performance can be attributed to the pronounced light harvesting efficiency, resulting from larger surface area and superior light scattering capability. The proposed CBT arrays fabricated using such simple protocol provides a prospect for a wide range of TiO_2 nanowires applications in energy conversion and storage devices.

Acknowledgments

The authors acknowledge the financial supports from the Program for New Century Excellent Talents in University (NCET-11-0533), the NSF of Guangdong Province (S2013030013474) and the Fundamental Research Funds for the Central Universities.

Appendix A. Supplementary data

Supplementary data related to this article can be found at http://dx.doi.org/10.1016/j.jpowsour.2014.02.107.

References

[1] B. O'Regan, M. Grätzel, Nature 353 (1991) 737–740.
[2] A. Yella, H.W. Lee, H.N. Tsao, C.Y. Yi, A.K. Chandiran, M.K. Nazeeruddin, E.W.G. Diau, C.Y. Yeh, S.M. Zakeeruddin, M. Grätzel, Science 334 (2011) 629–634.
[3] Q.F. Zhang, G.Z. Cao, Nano Today 6 (2011) 91–109.
[4] S. Yanagida, Y.H. Yu, K. Manseki, Acc. Chem. Res. 42 (2009) 1827–1838.
[5] L. Kavan, J.H. Yum, M. Grätzel, ACS Nano 5 (2011) 165–172.
[6] K.J. Jiang, K. Manseki, Y.H. Yu, N. Masaki, K. Suzuki, Y.L. Song, S. Yanagida, Adv. Funct. Mater. 19 (2009) 2481–2485.
[7] J.K. Koh, J. Kim, B. Kim, J.H. Kim, E. Kim, Adv. Mater. 23 (2011) 1641–1646.
[8] D.B. Kuang, S. Ito, B. Wenger, C. Klein, J.E. Moser, R. Humphry-Baker, S.M. Zakeeruddin, M. Grätzel, J. Am. Chem. Soc. 128 (2006) 4146–4154.
[9] X.J. Lu, F.Q. Huang, J.J. Wu, S.J. Ding, F.F. Xu, ACS Appl. Mater. Interfaces 3 (2011) 566–572.
[10] Z. Sun, J.H. Kim, Y. Zhao, D. Attard, S.X. Dou, Chem. Commun. 49 (2013) 966–968.
[11] J.Y. Liao, B.X. Lei, H.Y. Chen, D.B. Kuang, C.Y. Su, Energy Environ. Sci. 5 (2012) 5750–5757.
[12] W.Q. Wu, B.X. Lei, H.S. Rao, Y.F. Xu, Y.F. Wang, C.Y. Su, D.B. Kuang, Sci. Rep. 3 (2013) 1352.
[13] M. Lv, D. Zheng, M. Ye, J. Xiao, W. Guo, Y. Lai, L. Sun, C. Lin, J. Zuo, Energy Environ. Sci. 6 (2013) 1615–1622.
[14] O.K. Varghese, M. Paulose, C.A. Grimes, Nat. Nanotechnol. 4 (2009) 592–597.
[15] F.W. Zhuge, J.J. Qiu, X.M. Li, X.D. Gao, X.Y. Gan, W.D. Yu, Adv. Mater. 23 (2011) 1330–1334.
[16] D. Kuang, J. Brillet, P. Chen, M. Takata, S. Uchida, H. Miura, K. Sumioka, S.M. Zakeeruddin, M. Grätzel, ACS Nano 2 (2008) 1113–1116.
[17] M. Mojiri-Foroushani, H. Dehghani, N. Salehi-Vanani, Electrochim. Acta 92 (2013) 315–322.
[18] L.Y. Lin, C.Y. Chen, M.H. Yeh, K.W. Tsai, C.P. Lee, R. Vittal, C.G. Wu, K.C. Ho, J. Power Sources 243 (2013) 535–543.
[19] W.Q. Wu, H.S. Rao, Y.F. Xu, Y.F. Wang, C.Y. Su, D.B. Kuang, Sci. Rep. 3 (2013) 1892.
[20] Q. Huang, G. Zhou, L. Fang, L. Hu, Z.-S. Wang, Energy Environ. Sci. 4 (2011) 2145–2151.
[21] M.D. Ye, X.K. Xin, C.J. Lin, Z.Q. Lin, Nano Lett. 11 (2011) 3214–3220.
[22] W.-Q. Wu, J.-Y. Liao, H.-Y. Chen, X.-Y. Yu, C.-Y. Su, D.-B. Kuang, J. Mater. Chem. 22 (2012) 18057–18062.
[23] B. Liu, E.S. Aydil, J. Am. Chem. Soc. 131 (2009) 3985–3990.
[24] X.Y. Wang, Y. Liu, X. Zhou, B.J. Li, H. Wang, W.X. Zhao, H. Huang, C.L. Liang, X. Yu, Z. Liu, H. Shen, J. Mater. Chem. 22 (2012) 17531–17538.
[25] J.-Y. Liao, B.-X. Lei, Y.-F. Wang, J.-M. Liu, C.-Y. Su, D.-B. Kuang, Chem.—Eur. J. 17 (2011) 1352–1357.
[26] H. Wang, Y.S. Bai, Q.O. Wu, W. Zhou, H. Zhang, J.H. Li, L. Guo, Phys. Chem. Chem. Phys. 13 (2011) 6977–6982.
[27] F. Sauvage, F. Di Fonzo, A.L. Bassi, C.S. Casari, V. Russo, G. Divitini, C. Ducati, C.E. Bottani, P. Comte, M. Grätzel, Nano Lett. 10 (2010) 2562–2567.
[28] J. Qu, G.R. Li, X.P. Gao, Energy Environ. Sci. 3 (2010) 2003–2009.
[29] N.G. Park, J. van de Lagemaat, A.J. Frank, J. Phys. Chem. B 104 (2000) 8989–8994.
[30] J.Z. Chen, W.Y. Ko, Y.C. Yen, P.H. Chen, K.J. Lin, ACS Nano 6 (2012) 6633–6639.
[31] W.Q. Wu, Y.F. Xu, C.Y. Su, D.B. Kuang, Energy Environ. Sci. 7 (2014) 644–649.
[32] E. Scolan, C. Sanchez, Chem. Mater. 10 (1998) 3217–3223.
[33] W.Q. Wu, Y.F. Xu, H.S. Rao, C.Y. Su, D.B. Kuang, Nanoscale 5 (2013) 4362–4369.
[34] D.B. Kuang, C. Klein, Z.P. Zhang, S. Ito, J.E. Moser, S.M. Zakeeruddin, M. Grätzel, Small 3 (2007) 2094–2102.
[35] H.X. Wang, P.G. Nicholson, L. Peter, S.M. Zakeeruddin, M. Grätzel, J. Phys. Chem. C 114 (2010) 14300–14306.
[36] L. Dloczik, O. Ileperuma, I. Lauermann, L.M. Peter, E.A. Ponomarev, G. Redmond, N.J. Shaw, I. Uhlendorf, J. Phys. Chem. B 101 (1997) 10281–10289.